



UNIVERSITY OF LEEDS

This is a repository copy of *Structural design and verification of an innovative whole adaptive variable camber wing*.

White Rose Research Online URL for this paper:  
<http://eprints.whiterose.ac.uk/155098/>

Version: Accepted Version

---

**Article:**

Zhao, A, Zou, H, Jin, H et al. (1 more author) (2019) Structural design and verification of an innovative whole adaptive variable camber wing. *Aerospace Science and Technology*, 89. pp. 11-18. ISSN 1270-9638

<https://doi.org/10.1016/j.ast.2019.02.032>

---

© 2019 Published by Elsevier Masson SAS. This manuscript version is made available under the CC-BY-NC-ND 4.0 license <http://creativecommons.org/licenses/by-nc-nd/4.0/>.

**Reuse**

This article is distributed under the terms of the Creative Commons Attribution-NonCommercial-NoDerivs (CC BY-NC-ND) licence. This licence only allows you to download this work and share it with others as long as you credit the authors, but you can't change the article in any way or use it commercially. More information and the full terms of the licence here: <https://creativecommons.org/licenses/>

**Takedown**

If you consider content in White Rose Research Online to be in breach of UK law, please notify us by emailing [eprints@whiterose.ac.uk](mailto:eprints@whiterose.ac.uk) including the URL of the record and the reason for the withdrawal request.



[eprints@whiterose.ac.uk](mailto:eprints@whiterose.ac.uk)  
<https://eprints.whiterose.ac.uk/>

# 1 **Structural design and verification of an innovative whole adaptive variable camber wing**

2 Anmin Zhao<sup>a,b</sup>, Hui Zou<sup>a</sup>, Haichuan Jin<sup>a</sup>, Dongsheng Wen<sup>a</sup>

3 <sup>a</sup>National key Laboratory of Human Machine and Environment Engineering, Beihang  
4 University, Beijing, 100191, China

5 <sup>b</sup>National key laboratory of Computational Fluid Dynamics, Beihang University, Beijing,  
6 100191, China

7 **Abstract:** A whole adaptive variable camber wing (AVCW) equipped with an innovative  
8 double rib sheet (DRS) structure is experimentally and numerically studied in this work. The  
9 new design uses surface contact of DRS for force transmission of changeable camber wing  
10 instead of the traditional rigid hinge joint contact. The AVCW design allows the change of  
11 airfoil camber in a real-time process under different flight states and flight environment,  
12 which is of great interest to Unmanned Aerial Vehicle (UAV) applications.. Numerical results  
13 show that the used of the varying camber airfoil has better stalled characteristic and  
14 aerodynamic performance comparing with the Clark Y and AH-79-100C airfoil. . The flight-  
15 test experiments indicate that the total AVCW carrying the autonomous development adaptive  
16 control system (ACS) can further enhance UAV flight efficiency by 29.4% relative to Talon  
17 UAV. It suggests that using AVCW structural can increase the load capacity and improve  
18 flight efficiency, without increasing the overall structural weight, which is promising for  
19 future engineering application to the UAV field.

## 20 **Keywords:**

21 Double Rib Sheet (DRS), whole Adaptive Variable Camber Wing (AVCW), adaptive control  
22 system (ACS), flight efficiency;  
23

## 24 **1. Introduction**

25  
26  
27 Modern unmanned aerial vehicles (UAVs) are mainly designed to improve flight  
28 efficiency in multi-environment and multi-missions flight, in which an adaptive variable  
29 camber wing (AVCW) is the most essential [1-4]. Traditional AVCW design schemes are  
30

31 based on mechanical hinge transmission to accomplish the change of the wing camber. Such  
32 scheme, however, suffers many limitations as the hinge parts are heavy and the contact  
33 surfaces are point-contact, which results in not only a low operation efficient but also a stress  
34 concentration prone to structure failure.

35 Many attempts have been performed to overcome such problems. . In the 1980s',  
36 mission-adaptive wing technology research was launched by the National Advisory  
37 Committee for Aeronautics (NASA) and the Boeing Company. It was suggested that the  
38 traditional control surface could be replaced by a flexible composite material skin operated  
39 by a digital flight control system, leading to increased lift-drag ratio and delayed flow  
40 separation on the wing surface. However, the complexity and heavy weight of mechanistic  
41 drivers obstruct its practical application [5-7]. In recent years, many studies on variable  
42 camber morphing wing have been conducted regarding the aerodynamic and structure  
43 performance of conventional leading-edge and trailing-edge of wings, but the whole  
44 changeable camber wing has not been considered. Stanford et al. investigated the static and  
45 dynamic aeroelastic tailoring with variable camber control, and showed that the wing  
46 structural weight could be reduced by adopting variable camber continuous trailing-edge flap  
47 system with improved aeroelastic behavior of the wing [8] . It has been reported that a  
48 variable camber fowler flap aerodynamic performance with a double-sliding track can be used  
49 for general aviation aircraft. The maximum lift coefficient was increased by 6.6% and ratio of  
50 lift-to-drag was decreased by 7.58% relative to the reference conventional fowler flap model  
51 [9]. Moreover, some inconstant camber wing structure investigations have been effectively  
52 carried out by [10-13]. It was indicated that the variable camber morphing wing, which was  
53 composed of corrugated structures, was feasible by considering both numerical simulation  
54 and wind tunnel experimenta results. Furthermore, the deformation of morphing skin is  
55 determined by the bending stiffness of the material, which could be studied by the flexible  
56 shin stiffness requirement of variable wings.

57 Using new materials as an actuator of variable camber wings has received strong  
58 interest. The surface deformation of the UAVs altered by a piezoelectric ceramic structure was  
59 designed ( FlexSys Inc, U.S), resulting in reduced weight and increased cruise time of the  
60 UAVs [14]. Kota et al. investigated a flexible skin covering on the trailing edge of the wing

61 and realized the deformation of the wing by smoothly bending the flexible trailing edge [15].  
62 A variable camber wing was demonstrated by Beihang University (Li et al.,2009), which used  
63 the shape memory alloy (SMA) as the actuators to change wing camber. It was indicated that  
64 the average lift of the wing was improved by 20% in the wind tunnel experimental [16]. A  
65 variable trailing camber wing model was designed and made of SMA material, good  
66 actuation performance even in condition of external loads was demonstrated both numerically  
67 and experimentally [17]. A novel 0-Poisson's ratio cosine honeycomb support structure of  
68 flexible skin was proposed by Liu et al, which could reduce power consumption and driving  
69 force [18]. Li and Ang conducted an innovative adaptive variable camber compliant wing  
70 based on a new artificial muscle in [10]. The results showed that this method could design  
71 airfoils for this morphing wing in a quick and effective way. Some similar works also have  
72 been implemented by [19, 20]. Nevertheless, expensive smart materials and device instability  
73 restrict its wide engineering application.

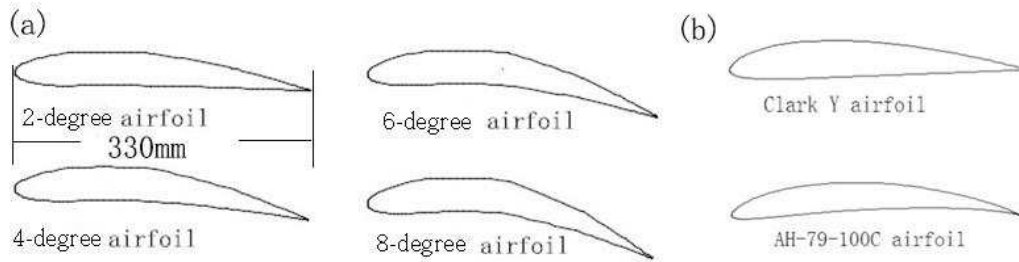
74 It is clearly from the review that that although extensive research has been performed  
75 for the aerodynamic, structure and material of the leading-edge or trailing-edge variable  
76 camber wings, the investigation of a whole AVCW has not yet been reported. This work aims  
77 to develop an innovative DRS structure that can realize the change of the whole camber of  
78 wing. 2D and 3D numerical simulations are conducted to investigate the influence of the  
79 camber change on the aerodynamic characteristics of the changeable airfoil and wing at  
80 different angles of attack. A prototype model of the complete varying camber wing is  
81 manufactured, and tested on ground and flight experiments. The flight-test results show that  
82 employing whole AVCW technology improves flight efficiency by ~ 29%.

83

## 84 **2. Structural model of the whole variable camber wing**

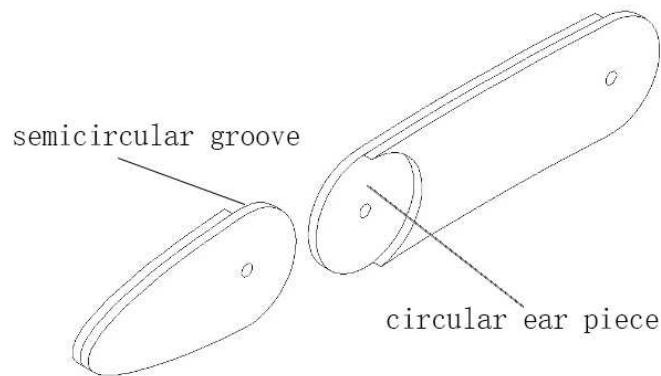
85 In order to define the deflection angle of the variable camber airfoil, a symmetrical airfoil,  
86 NACA 0012, is selected with the chord length  $L$  of 330mm [Fig. 1(a)]. A four-section airfoil  
87 is designed to obtain the whole camber change of airfoil in the proportion of 1:2:2:1.  
88 Illustrated in Figure 1(a), the four-typical state of airfoil is chosen to investigate the change  
89 of airfoil camber. The airfoil (NACA 0012) is modified to realize a smooth transition of  
90 airfoil to improve aerodynamics performance. To verify the flow advantages of variable

91 camber airfoil profile of 2D, Clark Y airfoil and AH-79-100C airfoil are selected for  
92 comparison, as shown in Figure 1-b.



93  
94 Figure 1. Schematic diagram of 2D airfoil: (a) 4-variable camber airfoil profiles, and (b)  
95 2-convention low-speed contrast airfoils.

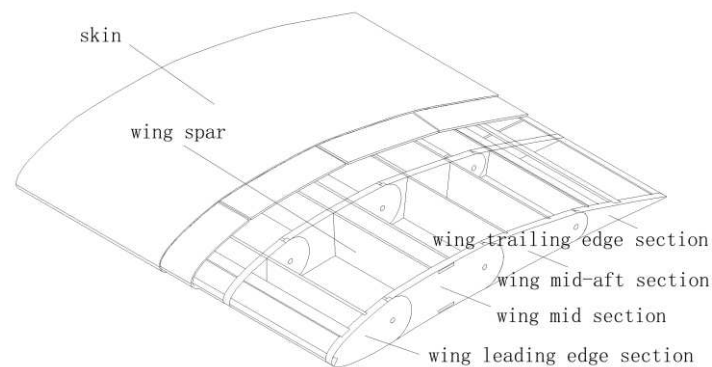
96  
97 A double rib sheet (DRS) structure is invented, as shown in Figure 2, to realize the  
98 overall wing camber change. The structural has one side of a semicircular groove, and the  
99 other side of a circular ear, both of which are in closely contact. Via this way, the geometry  
100 configuration of the complete wing rib is connected by four double rib sheets. It is clear that  
101 such mechanical structure design will not increase the weight of the entire wing structure. In  
102 addition, the load transfer between the sections of the wing rib structures is transformed into  
103 surface contact from the traditional point contact, which could not only avoids the problem of  
104 stress concentration, but also allows the structure to bear greater load.



105  
106 Figure 2. Double rib sheet structural model.

107 A schematic diagram of an innovation entire wing structure is presented in Figure3, with  
108 a total surface area of  $0.5\text{m}^2$ . The model is composed of wing rib, skin and wing spar, which is  
109 similar to the wing structure of general aviation aircraft, without the increase of additional  
110 weight except for the actuator. The wing rib model is composed of four separate wing

111 structural sections, which include the wing leading edge section, wing trailing edge section,  
112 wing mid-section and the wing mid-aft section, respectively. The overall wing camber change  
113 is obtained by the relative rotation between the wing rib structure sections. Compared with  
114 traditional control mode, the variable camber wing can change the complete wing camber  
115 when the state and conditions of flying are varied. The test experiment of the whole  
116 changeable camber wing on the ground is shown in the supplementary material. It is  
117 known that conventional aircraft is designed to reach optimal performance characteristics  
118 only for a single mission. However, changes in the flight states and flight environment of  
119 UAV are inevitable, and the traditional fixed wing structure could not achieve a multi-  
120 missions optimal flight. . The design of AVCW shall address this issue by allowing real-time  
121 change of wing position by the active control system (ACS). In this way, the airfoil of the  
122 wing is always adjusted to the optimum state based on different flight states and flight  
123 environment. It is expected that comparing to the variable leading-edge camber wing or  
124 variable trailing-edge camber wing structure, employing the whole AVCW technology could  
125 improve further UAV aerodynamic characteristics and flight efficiencies, as shown by both  
126 numerical modelling and flight experiments below.



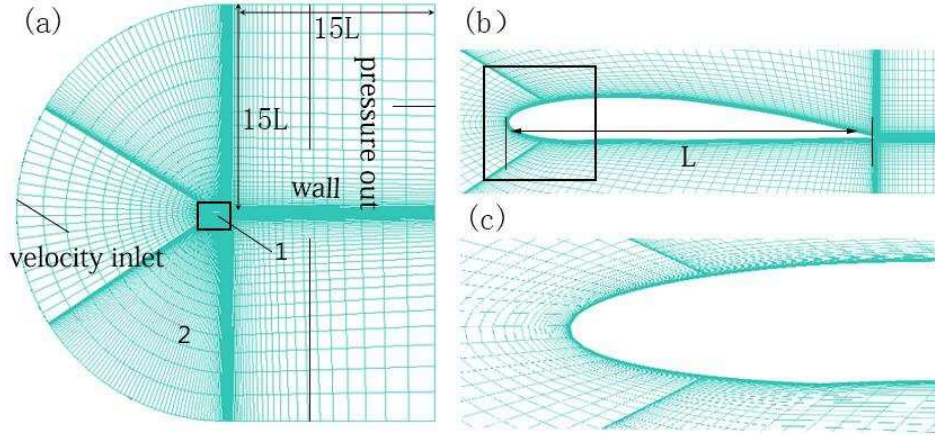
127  
128 Figure 3. Variable camber wing structure model  
129

### 130 3. Numerical simulation

#### 131 3.1 D grid generation and boundary conditions of AVCW

132 A C-type structured grid is adopted in the ICEM CFD 15.0 [21] to discretize the flow field  
133 around airfoil two-dimensional model, as illustrated in Figure 4. The computational domain is  
134 selected to be big enough to avoid the influence of far-field boundary conditions on the flow

135 characteristic of the model. The mesh extends to 15L from airfoil surface to the far-field  
 136 boundary, i.e., the boundary length is 15L from upstream, downstream, the upper and lower  
 137 boundaries respectively. Figure 4(a) shows the structured grid for the integral calculation  
 138 domain, which is divided into two parts: 1(airfoil) and 2(far-field) for the inner and outer  
 139 mesh, respectively. Figure 1(b) and 1(c) show an enlarged view of the airfoil profile and the  
 140 quality of the grid is 0.76~0.866.



141

142 Figure 4. Schematic of the computation mesh and boundary conditions

143 The far-field boundary conditions are set as follows: the inlet boundary is the velocity  
 144 inlet; the upper and lower boundary is the no-slip wall; and the out boundary is defined as  
 145 pressure out, shown in Figure 4-a. The Reynolds number is given by

146 
$$\text{Re} = \frac{\rho L U_{\infty}}{\mu} \quad (1)$$

147 Where  $\rho$ ,  $\mu$ ,  $U_{\infty}$  and  $L$  are air density 1.225 kg/m<sup>3</sup>, air kinematic viscosity coefficient  
 148  $1.7894 \times 10^{-5}$  kg/(mgs), the free-velocity 18 m/s, and the chord length of airfoil 0.33m,  
 149 respectively.

150 Based on the equation (1) and above constant, the Reynolds number is calculated as  
 151 406508. The drag and lift are parallel and perpendicular to the far-field free stream. The  
 152 corresponding lift and drag coefficient can be given as

153 
$$C_l = \frac{F_y}{0.5 \rho U_{\infty}^2 S} \quad (2)$$

154 
$$C_d = \frac{F_x}{0.5 \rho U_{\infty}^2 S} \quad (3)$$

155 Where  $C_l$  is the lift coefficient,  $C_d$  is the drag coefficient,  $S$  is the area of the wing,  $F_x$

156 and  $F_y$  are the drag and lift, respectively.

157 In order to ensure grid independence, four types of mesh with different grid density are  
158 employed to investigate lift and drag coefficients for a 2-degree airfoil shown in Figure 1  
159 with the angles of attack of  $6^\circ$  and  $10^\circ$  respectively. The simulation results in Table 1 show  
160 that the differences of drag and lift coefficients are within 4% between types 2 and 3. With  
161 further increase of grid cell density, the difference can be reduced to less than 3%.  
162 However for the consideration of both simulation accuracy and simulation time constrains,  
163 the grid density of type 2 is chosen in this work.

164 Table 1. Mesh independence study for variable camber airfoil at  $Re=406508$  and angle of  
165 attack of  $6^\circ$  and  $10^\circ$

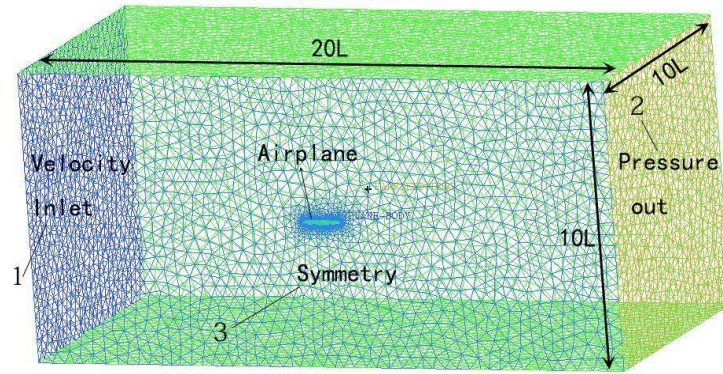
Type	Number of cells	Angle of attack $6^\circ$		Angle of attack $10^\circ$	
		$C_L$	$C_d$	$C_L$	$C_d$
1	15000	1.1152	0.78951	1.3125	0.4352
2	39500	1.1387	0.08078	1.3413	0.1447
3	88000	1.1806	0.08352	1.3822	0.1421
4	250000	1.1625	0.08452	1.3652	0.1435

166 The normal velocity of boundary layer is very substantial in the adjacent airfoil region,  
167 and the boundary grid Y spacing value set is critical to calculate the flow field of the near  
168 wall region. In this study, NACA  $Y^+$  wall distance estimation online is adopted, and the  
169 height of the first layer grid is calculated to 0.000128m. The universal computational fluid  
170 dynamics solver employed is the Spalart-Allmaras model (SA) [22]. In order to obtain an  
171 analogy wind tunnel tests condition, a no-slip boundary condition of the airfoil surface is  
172 applied.

### 173 3.2 3D grid generation and boundary conditions of AVCW

174 The unstructured grid is adopted in the ICEM CFD 15.0 [21] to discretize the flow field  
175 around the three-dimensional model, as is shown in Figure 5, with a size of the  
176 computational domain of  $20L \times 10L \times 10L$  in the X, Y and Z direction, respectively. According  
177 to the demand of meshing refining in the region of the wing, the prism grid parameters are  
178 employed. The reference signs 1, 2 and 3 in Figure 5 represent the velocity inlet, pressure  
179 outlet and symmetric boundary conditions, respectively.





180

181

Figure 5. Symmetric computational domain grid and boundary conditions

182

183

184

185

186

187

188

To verify grid independence, four cases of mesh densities are adopted to compute the lift and drag coefficients. Based on 3-degree of the variable camber of wing in Figure 5(b), the Reynolds number ( $Re$ ) is calculated as 406508 at angles of attack of  $6^\circ$  and  $10^\circ$ , respectively. The numerical results are summarized in Table 2, which indicate that the differences between cases 2 and 3, and between cases 3 and 4 are less than 2%. To achieve a relatively high resolution of grid, the mesh of case 2 is utilized for the present numerical simulation and the total number of cells and nodes are 36062701 and 4527750, respectively.

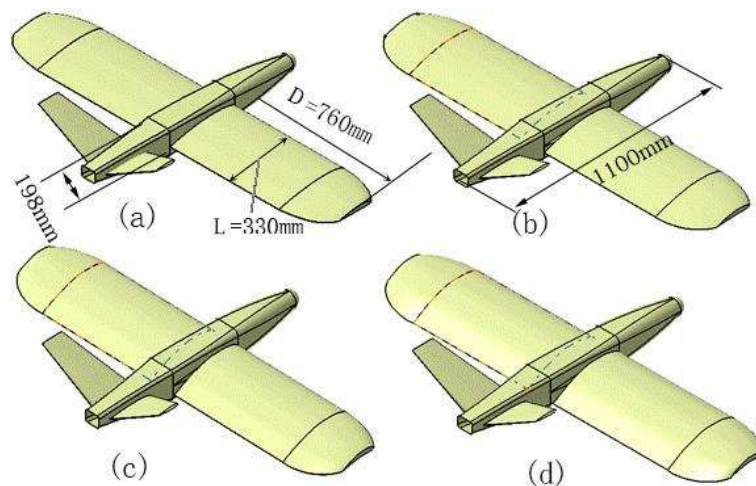
189

190

191

192

This step allows us to obtain more accurate estimations of the flow characteristics as well as to make a preparation for flight test. Four types of whole variable camber wing aircraft models are selected, which are defined as 1-degree wing model, 3-degree wing model, 5-degree wing model and 7-degree wing model, respectively.



193

194

195

196

Figure 6. Four models of the variable camber wing aircraft. (a) 1-degree wing model, (b) 3-degree wing model, (c) 5-degree wing model, (d) 7-degree wing model ( $D$ : Half of span)  
Table 2. Research on grid independence for variable camber aircraft at  $Re=406508$  and angle

Case	Number of cells	Angle of attack $6^\circ$		Angle of attack $10^\circ$	
		$C_L$	$C_d$	$C_L$	$C_d$
1	15000000	0.682	0.11051	0.826	0.4362
2	36062701	0.629	0.10458	0.778	0.1320
3	58500000	0.635	0.108352	0.786	0.1421
4	85250000	0.621	0.108452	0.782	0.1315

198

#### 4. Aerodynamic performance of AVCW

199

200

201

202

203

204

205

##### 4.1 2D aerodynamic characteristics

206

207

208

209

210

211

212

213

214

215

216

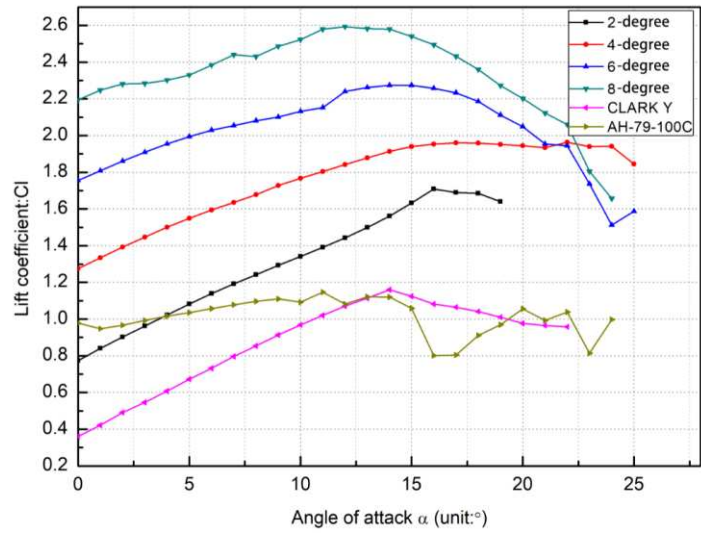
217

218

The flow characteristics of flow field of changeable camber wing are computed with two-dimensional and three-dimension incompressible continuous equations. According to Navier-Stokes (N-S) equations, a series of numerical simulations are performed under different initial conditions to investigate the aerodynamic performance of the variable camber airfoil and wing, as below.

Based on the research purpose, four kinds of design variable camber airfoil and two types of conventional airfoil are selected, as described in Figure 1. The angle of attack varies from  $0^\circ$  to  $25^\circ$ , of which simulation results are shown in Figure 7-9.

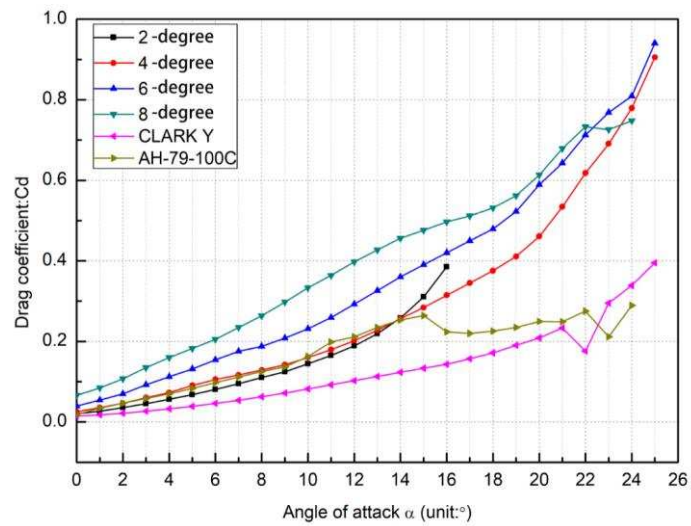
Figure 7 shows that the aerodynamic performance greatly affects the lift coefficient owing to the change of the airfoil camber. The lift coefficient gradually increases with the increase of airfoil camber at the same angles of attack, which can be observed in Figure 7. In addition, it can be discovered that the camber is beneficial to enhance the lift performance when the angle of attack is smaller than  $15^\circ$ . With further increase of the angle of attack, the lift coefficient gradually decreases, which may cause flow separation due to the unsteady vortex of the near airfoil surface. Therefore,  $15^\circ$  corresponds to the critical angle of attack in the numerical results. In general, the variable camber airfoil has a stall angle of attack at about  $15^\circ$  and is larger than those of the Clark Y and AH-79-100C airfoil, leading to improved lift aerodynamic characteristics.



219

220

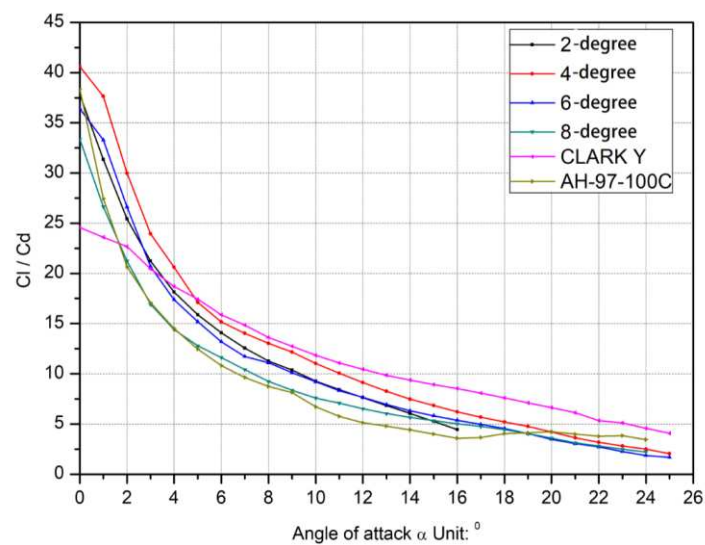
Figure 7. Lift coefficient distribution of 2D different variable airfoils and angle of attack



221

222

Figure 8. Drag coefficient distribution of 2D different variable airfoils and angle of attack



223

224

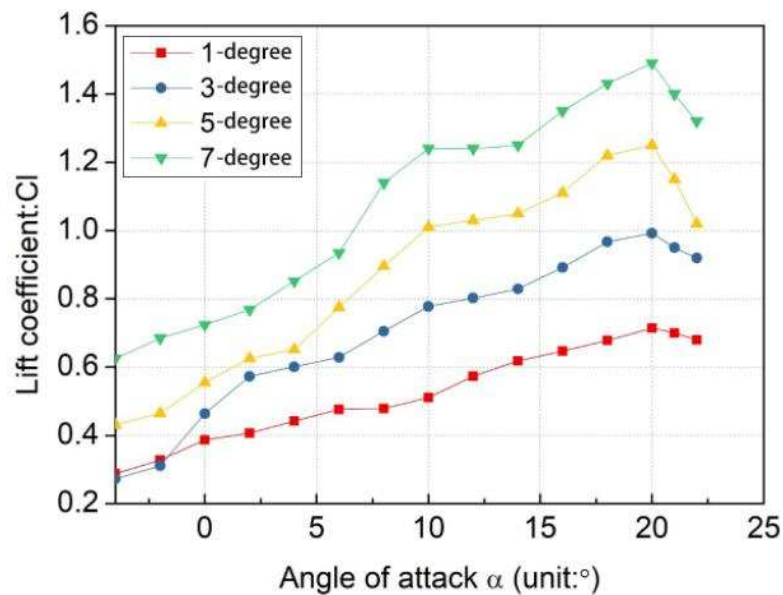
Figure 9. Pole curve of 2D different variable camber airfoils and angle of attack

225 From Figure 8, it can be seen that the drag coefficient of airfoil also increases with the  
 226 growth of the angle of attack, which mainly owes to the excessive ??? camber for the design  
 227 airfoil. It also means that further modify variable camber airfoil is needed in future work. As  
 228 shown in Figure 9, while the angle of the airfoil camber is smaller than 4-degree, it is in favor  
 229 of enhancing the ratio of lift to drag. Compared with Clark Y and AH-79-100C airfoil,  
 230 appropriate airfoil camber design strengthens aerodynamic performance. However, the greater  
 231 initial camber angle of airfoil deteriorates the aerodynamic performance. It is mainly caused  
 232 by laminar-turbulence transition around the airfoil, eventually leading to decreased lift  
 233 coefficient and increased drag coefficient. On condition that the numerical simulation results  
 234 in this work, 15° angle of attack is recommended to apply for the design variable camber  
 235 airfoil.

236

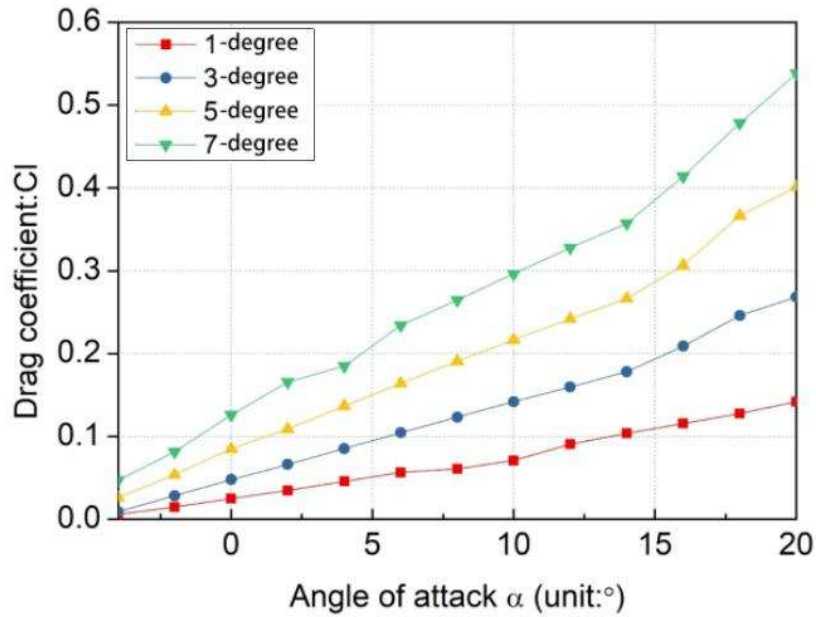
### 237 4.2 3D aerodynamic characteristics

238 In order to validate the aerodynamic performance of varying camber wing in three-  
 239 dimensional configurations, four types of changeable camber wing are chosen and computed.  
 240 To enhance the efficiency and accuracy of calculation, the variable camber wing aircraft  
 241 model is simplified to a half model, but the tail is included. As shown in Figure 10 -11, the  
 242 camber change of wing has a significant effect on the aerodynamic performance.



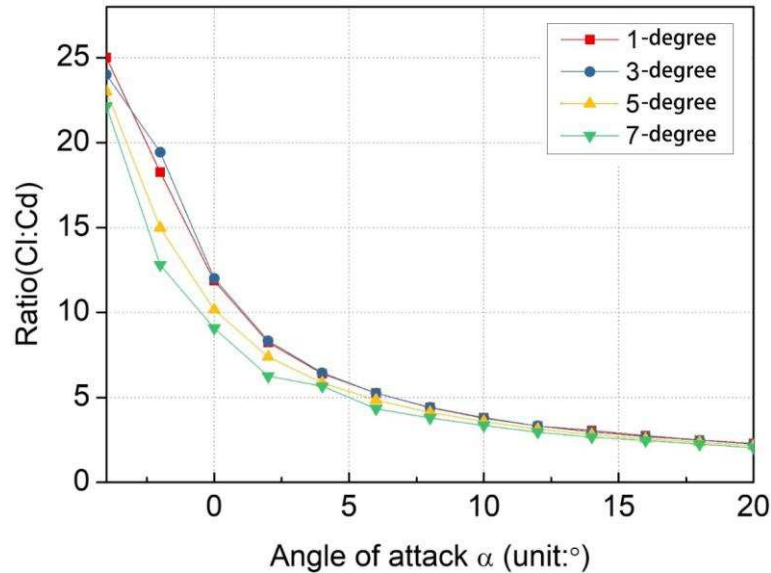
243

244 Figure 10. The effect of lift coefficients with different 3D wing camber and angle of attack



245

246 Figure 11. The effect of drag coefficients with different 3D wing camber and angle of attack



247

248 Figure 12. The effect of the pole curve with different 3D wing camber and angle of attack

249 Figure 10-12 show the lift coefficient, drag coefficient and pole curve distribution of  
 250 variable camber wing from  $-2^\circ$  to  $20^\circ$  of angle of attack, respectively. Compared with 2D  
 251 numerical results, the trend of the curve distribution is similar. Adjustable camber can  
 252 effectively control lift coefficient under three-dimensional wing situations. However, it is  
 253 noteworthy that there are a few distinctions here. First of all, the stall angle of attack of the  
 254 entire variable camber wing is about  $18^\circ$ , greater than the result from 2D simulation in  
 255 Figure 7, which is mainly due to the impact of the tail and the overall layout on the flow  
 256 characteristics of UAV. It also can be seen that the lift coefficient is smaller compared with the

257 airfoil numerical results (Fig. 7) and the drag coefficient is similar (Fig. 8 and Fig. 11) in the  
258 range from  $0^\circ$  to  $20^\circ$  angle of attack. Figure 12 shows that when the camber is lower than 3-  
259 degree, reducing the camber of the wing can increase the ratio of lift to drag. Taking into  
260 consideration the above-mentioned error factors, two-dimensional and three-dimensional  
261 models of the calculation results can be used to as a reference for design and flight test of  
262 AVCW UAV.

263

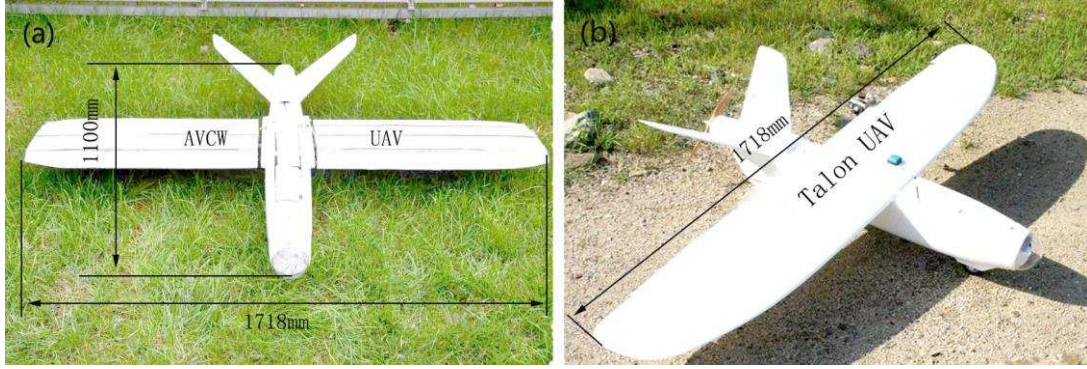
## 264 **5. AVCW aircraft manufacture and ground test**

265 In order to verify the flight advantage of the complete changeable camber wing, an electric  
266 prototype model is manufactured with take-off weight of four kilograms. In the design of the  
267 entire varying camber wing aircraft, a widely used Talon UAV (X-UAV fat fixed-wing aircraft)  
268 fuselage is adopted for the purpose of easy comparison and reduced error of production.  
269 Two experimental prototype models are built, one of which is the combination of the Talon  
270 UAV fuselage and the whole variable camber wing (see Figure 13a), and the other is the  
271 unmodified Talon UAV fuselage and wing (see Figure 13b). It is remarkable that the above  
272 variable camber wing design parameters are identical with Talon UAV wing. The detail  
273 parameters are shown in Table 3.

274 The processes of UAV manufacture and assembly are demonstrated as follows, which are  
275 presented in detail in the supporting material.

276 (1) The changeable camber wing part is designed in AutoCAD software, (2) The wing rib,  
277 wing spar, DRS structure, skins and other components are cut by laser, (3) The variable  
278 camber wing and the fuselage are assembled, (4) The steering gear, motor, battery, and  
279 adaptive flight control system are installed, and (5) The whole AVCW aircraft testing on  
280 ground is completed.





281

282 Figure 13. The flight test of whole AVCW aircraft and traditional fixed-wing Talon aircraft, (a)

283

AVCW UAV, and (b) Talon UAV

284

Table 3 General parameters of the electric prototype model

Item	value
Wing span / mm	1718
Wing area / m <sup>2</sup>	0.5
Take-off weight / kg	4
Fuselage length / mm	1100

285

286

287

288

289

290

291

292

293

294

## 6. Flight-test validation

295

296

297

298

299

It is worth noting that the variable camber wing structure is made of light aircraft wood structure, with thickness of 1mm, 2mm, 3mm respectively. In addition, the skin is arranged in a way like overlapping fish scales to obtain a smooth aerodynamic shape. In order to reach the flexible flight for changeable camber wing aircraft, the adaptive flight control system is developed based on the PX4 and Mission planner secondary development. In the case of the ACS is not equipped, the expense of the whole variable camber wing prototype model is less than 500 \$. The production and fabrication costs of AVCW UAV can be significantly reduced in the future during mass production.

Noticeably, it is of great significance to verify the validity of numerical simulation results, the effectiveness of the performance indicators in design and reasonability of structural design among flight experiment. Thereby, an X-UAV and fixed-wing aircraft and a nearly similar constant wing camber aircraft based on the AVCW UAV adjusted by the ACS, are chosen for the flight trial result. First of all, the equivalent configuration parameters of UAV are

300 adopted. Besides, two identical standard 2000 mAh batteries, battery charger and voltmeter  
301 are prepared before the flight test. In the same flying state, including straight line of 20 meters  
302 per second and uniform airline, a 10-minutes flight test is carried out. The voltage of the  
303 battery is obtained based on the results of five flight experiments for every airplane model.  
304 However, it should be noted here that the voltage of the battery before the flight is 16.5V and  
305 the battery are fully charged for repeatability experiment. The results indicate that the average  
306 voltage drop of 5 flight trials for different aircraft prototypes is 0.8V and 0.78V, respectively.  
307 The above flight-test results are in good quantitative agreement. In general, the changeable  
308 camber wing design is considered to be believable.

309 To analyze the real-time flight characteristics of AVCW aircraft, two groups comparison  
310 flight-test experiments are conducted, in which one group of flight experiment are the AVCW  
311 UAV and X-UAV fat fixed-wing aircraft, and the other group of tests are AVCW UAV and  
312 constant camber state when the camber of the variable camber wing aircraft is defined as 3-  
313 degree, one of which the AVCW aircraft flight test is presented in the Supporting Material.

314

## 315 **7.1 Experiment 1**

316 The experimental system is a comparative trial between an X-UAV fat fixed-wing aircraft and  
317 an AVCW UAV. Flight tests are attained with the following procedure. Firstly, two 5000 mAh  
318 4S batteries of the same model, battery charger, a voltmeter and transmitter power control  
319 (Futaba T4YF-2.4GHz transmitter) are provided. Using a calibrated voltmeter, the voltage of  
320 the battery is measured to 16.4V and 16.5V, correspondingly, which is utilized to provide  
321 power for the AVCW UAV and X-UAV fat fixed-wing aircraft. Before the experiment is  
322 performed, the ACS is debugged, and three types of flight cruise models are set.

323 Table 4 displays the details of the experiment conditions, including the cruise model is  
324 12m/s, 14m/s and 16m/s and cruise time is 5 minutes. In a similar flight environment, this  
325 contains the flight altitude, atmospheric temperature, atmospheric humidity and airflow, etc.  
326 Noted that five flight experiments for every aircraft prototype model are carried out and the  
327 battery is fully charged for repeatability experiment. The flight-test results reveal that the  
328 mean voltage drop of the battery is 1.2V in the adaptive flight state. Whereas for a X-UAV  
329 fat fixed-wing aircraft under the same flight missions, the voltage drop is 1.7V. Table 4.



Test	Aircraft type	Number of Tests	Cruise setting	Voltage drop	Dissipative energy
Test 1	AVCW	5	5min, 12m/s	1.2V	21600000J
			5min, 14m/s		
			5min, 16m/s		
Test 2	Talon	5	5min, 12m/s	1.7V	30600000J
			5min, 14m/s		
			5min, 16m/s		

331 Based on Test 1 and Test 2, the complete changeable camber wing in flexible flight  
332 condition can save electricity about 0.5V relative to the X-UAV fat fixed-wing aircraft. It can  
333 be estimated that the whole adaptive variable camber flight improves the flight efficiency by  
334 29.4% compared with X-UAV fat fixed-wing aircraft under the same flight mission. The  
335 whole AVCW technology breaks the constraints of energy and power systems for cruise time.  
336 The application of this technology may promote the technical revolution in the field of fixed-  
337 wing UAV, which is of great significance to the development of the UAV industry and has a  
338 high scientific research value.

339

## 340 7.2 Experiment 2

341 The experimental system setting and results are presented in Table 5. Effects on the flight  
342 performance for the comparative experiment of the whole AVCW and 3-degree constant  
343 camber wing are investigated. Based on Table 5, two 2000mAh batteries of the uniform  
344 capacity are applied. The cruise velocity of Test 1 and Test 2 is about 20 m/s under the same  
345 flight states. It should be noted that five flight trials for prototype model are performed and  
346 the battery is fully charged for repeatable experiment.

347 The experimental results are shown as follows: when ACS is adopted, the cruise time of  
348 whole AVCW aircraft is longer than that of fixed wing camber at 3-degree. Because the UAV  
349 is equipped with an ACS, it can achieve real-time change of for wing camber during the entire  
350 flight to accomplish the minimum flight drag. It can be observed that the results show the

351 average cruise time of the whole AVCW wing and 3-degree fixed camber wing are 45 minutes  
352 and 35 minutes, respectively. Compared with the Table 5, a conclusion can be drawn: adding  
353 the ACS to UAV can increase the flight efficiency by 28.6%.

354

355 Table 5. Comparison of flight test of adaptive camber aircraft and 3-degree constant wing

356

357

358

---

Test	Aircraft type	Number of tests	Power supply	Cruise setting	Cruise time
Test 1	AVCW	5	2000mAh	20m/s	45minutes
Test 2	3-degree constant camber wing	5	2000mAh	20m/s	35minutes

---

## 359 7. Conclusions

360 In the paper, an innovative double rib sheet structure is proposed to control the position of a  
361 whole camber of the wing by a relative rotational motion of the DRS groove contact surface.  
362 Numerical simulation is applied to investigate the effect of varying camber airfoil and wing  
363 on the aerodynamic performance of UAV. In order to realize further flight experiment study,  
364 the whole changeable camber wing prototype model with an ACS is manufactured. Two  
365 groups of controlled flight-test experiment are conducted to demonstrate aerodynamic  
366 performance benefits of AVCW UAV. The following conclusions can be drawn as

367 1) An innovative DRS structure is invented, which accomplishes the change of the whole  
368 variable camber wing without increasing the overall structural weight of the wing except for  
369 the actuating device.

370 2) The load transfer mode of the new design of variable camber wing structure is groove  
371 surface contact, which allows the structure to reach enormous capacity for loads.

372 4) As compared with Clark Y airfoil and AH-79-100C airfoil, adjustable camber airfoils  
373 have shown better aerodynamic performance and stalled characteristics.

374 5) The flight experiment (experiment 1) results show that comparison with the design  
375 scheme of traditional fixed wing of Talon UAV, the whole AVCW technology improves  
376 aircraft flight efficiency by 29.4%.

377 6) Using the experimental setup and programs described in trial 2, the results show that  
378 adding the ACS to UAV improves the flight efficiency by 28.6%.

379 Further study is necessary to explore the appropriate number of wing rib sections and  
380 investigate the effects of the relative rotation angle between different sections on aerodynamic  
381 performance of the whole AVCW UAV.

382

### 383 **Acknowledgement**

384 The work was supported by the Innovation and Entrepreneurship Foundation No. XXXXXX  
385 to the Beihang university, and the Beihang Aviation Innovation Practice Base.

386

### 387 **Reference**

388 [1] T. Mihetec, Utilization of the Flexible Airspace Structure in the Flight Efficiency

389 Optimisation, Hrvatska znanstvena bibliografija i MZOS-Svibor, DOI (2012).

390 [2] D. Koch, Quiet, efficient fans for space flight: An overview of NASA's technology

391 development plan, Journal of the Acoustical Society of America, 127 (2010) 1838-1838.

392 [3] M. Bashir, P. Rajendran, Morphing Wing Technologies, 2017.

393 [4] W.H. Su, S.S.M. Swei, G.M.G. Zhu, Optimum Wing Shape of Highly Flexible Morphing

394 Aircraft for Improved Flight Performance, J. Aircr., 53 (2016) 1305-1316.

395 [5] S. POWERS, L. WEBB, E. FRIEND, W. LOKOS, Flight test results from a supercritical

396 mission adaptive wing with smooth variable camber, 28th National Heat Transfer

397 Conference, 1992, pp. 4101.

398 [6] J.N. Kudva, Overview of the DARPA Smart Wing Project, J.intell.mater.syst.struct, 15

399 (2004) 261-267.

400 [7] J.N. Kudva, B.P. Sanders, J.L. Pinkertonflorance, E. Garcia, Overview of the

401 DARPA/AFRL/NASA Smart Wing Phase II program, Proc Spie, 4332 (2001) 383-389.

- 402 [8] B.K. Stanford, Static and Dynamic Aeroelastic Tailoring with Variable-Camber Control,  
403 Journal of Guidance Control and Dynamics, 39 (2016) 2522-2534.
- 404 [9] Y. Tian, T. Wang, P. Liu, P. Feng, Aerodynamic/mechanism optimization of a variable  
405 camber Fowler flap for general aviation aircraft, Sci. China-Technol. Sci., 60 (2017) 1144-  
406 1159.
- 407 [10] H.D. Li, H.S. Ang, Preliminary airfoil design of an innovative adaptive variable camber  
408 compliant wing, J. Vibroeng., 18 (2016) 1861-1873.
- 409 [11] W. Yin, Stiffness requirement of flexible skin for variable trailing-edge camber wing, Sci.  
410 China-Technol. Sci., 53 (2010) 1077-1081.
- 411 [12] T. Yokozeki, A. Sugiura, Y. Hirano, Development of Variable Camber Morphing Airfoil  
412 Using Corrugated Structure, J. Aircr., 51 (2014) 1023-1029.
- 413 [13] F. Gandhi, P. Anusonti-Inthra, Skin design studies for variable camber morphing airfoils,  
414 Smart Materials & Structures, 17 (2008).
- 415 [14] H. Zhu, W.D. Liu, C.S. Zhao, Morphing Aircraft and Its Morph-driving Techniques,  
416 Machine Building & Automation, DOI (2010).
- 417 [15] S. Kota, R. Osborn, G. Ervin, D. Maric, P. Flick, D. Paul, Mission Adaptive Compliant  
418 Wing – Design , Fabrication and Flight Test Mission Adaptive Compliant Wing, DOI (2006).
- 419 [16] L. Jun, Q. Yanhua, B. Tao, Y. Zhehui, L. Yan, Development of a morphing wing with  
420 adaptive capability, Acta Aerodynamica Sinica, 27 (2009) 505-508.
- 421 [17] S. Barbarino, R. Pecora, L. Lecce, A. Concilio, S. Ameduri, L. De Rosa, Airfoil  
422 Structural Morphing Based on SMA Actuator Series: Numerical and Experimental Studies,  
423 Journal of Intelligent Material Systems and Structures, 22 (2011) 987-1004.
- 424 [18] W. Liu, H. Zhu, S. Zhou, Y. Bai, Y. Wang, C. Zhao, In-plane corrugated cosine  
425 honeycomb for 1D morphing skin and its application on variable camber wing, Chinese  
426 Journal of Aeronautics, 26 (2013) 935-942.
- 427 [19] W. Yin, L. Liu, Y. Chen, J. Leng, Variable camber wing based on pneumatic artificial  
428 muscles, in: J. Leng, A.K. Asundi, W. Ecke (Eds.) Second International Conference on Smart  
429 Materials and Nanotechnology in Engineering2009.
- 430 [20] W. Yin, L. Liu, Y. Chen, Y. Liu, J. Leng, Pneumatic artificial muscle and its application  
431 on driving variable trailing-edge camber wing, in: M.B. McMickell, K.M. Farinholt (Eds.)

432 Industrial and Commercial Applications of Smart Structures Technologies 20102010.

433 [21] I. ANSYS, ANSYS FLUENT User's Guide DOI (2011).

434 [22] A. Fluent, ANSYS FLUENT 14.5 Theory Guide, DOI (2012).

435